Research Article | Vol. 26, No. 14 | 9 Jul 2018 | OPTICS EXPRESS 18448
Optics EXPRESS

High-efficiency energy transfer in perovskite heterostructures

YILING SONG,[1,3] CONG ZHANG,[1,3] WEIWEI LIU,[1,*] XIAOHONG LI,[1] HUA LONG,[1] KAI WANG,[1] BING WANG,[1] AND PEIXIANG LU[1,2]

[1]*Wuhan National Laboratory for Optoelectronics and School of Physics, Huazhong University of Science and Technology, Wuhan 430074, China*
[2]*Laboratory for Optical Information Technology, Wuhan Institute of Technology, Wuhan 430205, China*
[3]*Contributed equally to this work*
[*]*lwhust@hust.edu.cn*

Abstract: Here, we report the energy transfer in $(PEA)_2PbI_4$/$MAPbBr_3$ perovskite heterostructures. Under two-photon excitation, the photoluminescence (PL) emission of the $(PEA)_2PbI_4$ flake is nearly completely quenched, while that of the $MAPbBr_3$ microplate is greatly increased (6.5 folds higher) in the heterostructure. The opposite variation character of the PL emissions is attributed to the radiative energy transfer from the $(PEA)_2PbI_4$ flake to the $MAPbBr_3$ microplate. The radiative energy transfer occurs on an ultrafast timescale with a high efficiency (~100%). In addition, a strongly thickness- and wavelength-dependent interlayer interaction is observed under one-photon excitation. This work advocates great promise for revealing the interlayer interaction of perovskite heterostructures and developing high-performance optoelectronic devices.

OCIS codes: (250.0250) Optoelectronics; (250.4390) Nonlinear optics, integrated optics; (250.5230) Photoluminescence; (190.4180) Multiphoton processes; (260.2160) Energy transfer.

References and links

1. F. Ceballos, M. G. Ju, S. D. Lane, X. C. Zeng, and H. Zhao, "Highly efficient and anomalous charge transfer in van der Waals trilayer semiconductors," Nano Lett. **17**(3), 1623–1628 (2017).
2. A. Raja, A. Chaves, J. Yu, G. Arefe, H. M. Hill, A. F. Rigosi, T. C. Berkelbach, P. Nagler, C. Schüller, T. Korn, C. Nuckolls, J. Hone, L. E. Brus, T. F. Heinz, D. R. Reichman, and A. Chernikov, "Coulomb engineering of the bandgap and excitons in two-dimensional materials," Nat. Commun. **8**, 15251 (2017).
3. W. Liu, Y.-N. Zhu, M. Liu, B. Wen, S. Fang, H. Teng, M. Lei, L.-M. Liu, and Z. Wei, "Optical properties and applications for MoS_2-Sb_2Te_3-MoS_2 heterostructure materials," Photon. Res. **6**(3), 220–227 (2018).
4. X. Li, S. Lin, X. Lin, Z. Xu, P. Wang, S. Zhang, H. Zhong, W. Xu, Z. Wu, and W. Fang, "Graphene/h-BN/GaAs sandwich diode as solar cell and photodetector," Opt. Express **24**(1), 134–145 (2016).
5. Y. Lee, J. Kwon, E. Hwang, C. H. Ra, W. J. Yoo, J. H. Ahn, J. H. Park, and J. H. Cho, "High-performance perovskite-graphene hybrid photodetector," Adv. Mater. **27**(1), 41–46 (2015).
6. Z. Wu, X. Li, H. Zhong, S. Zhang, P. Wang, T. H. Kim, S. S. Kwak, C. Liu, H. Chen, S.-W. Kim, and S. Lin, "Graphene/h-BN/ZnO van der Waals tunneling heterostructure based ultraviolet photodetector," Opt. Express **23**(15), 18864–18871 (2015).
7. S. Bettis Homan, V. K. Sangwan, I. Balla, H. Bergeron, E. A. Weiss, and M. C. Hersam, "Ultrafast exciton dissociation and long-lived charge separation in a photovoltaic pentacene-MoS_2 van der Waals heterojunction," Nano Lett. **17**(1), 164–169 (2017).
8. A. Boulesbaa, K. Wang, M. Mahjouri-Samani, M. Tian, A. A. Puretzky, I. Ivanov, C. M. Rouleau, K. Xiao, B. G. Sumpter, and D. B. Geohegan, "Ultrafast charge transfer and hybrid exciton formation in 2D/0D heterostructures," J. Am. Chem. Soc. **138**(44), 14713–14719 (2016).
9. W. Xu, W. Liu, J. F. Schmidt, W. Zhao, X. Lu, T. Raab, C. Diederichs, W. Gao, D. V. Seletskiy, and Q. Xiong, "Correlated fluorescence blinking in two-dimensional semiconductor heterostructures," Nature **541**(7635), 62–67 (2017).
10. P. K. Nayak, Y. Horbatenko, S. Ahn, G. Kim, J. U. Lee, K. Y. Ma, A. R. Jang, H. Lim, D. Kim, S. Ryu, H. Cheong, N. Park, and H. S. Shin, "Probing evolution of twist-angle-dependent interlayer excitons in $MoSe_2$/WSe_2 van der Waals heterostructures," ACS Nano **11**(4), 4041–4050 (2017).
11. Q. Fang, Q. Shang, L. Zhao, R. Wang, Z. Zhang, P. Yang, X. Sui, X. Qiu, X. Liu, Q. Zhang, and Y. Zhang, "Ultrafast charge transfer in perovskite nanowire/2D transition metal dichalcogenide heterostructures," J. Phys. Chem. Lett. **9**(7), 1655–1662 (2018).

#327058 https://doi.org/10.1364/OE.26.018448
Journal © 2018 Received 27 Mar 2018; revised 1 Jun 2018; accepted 27 Jun 2018; published 3 Jul 2018

Optics EXPRESS

12. D. Kozawa, A. Carvalho, I. Verzhbitskiy, F. Giustiniano, Y. Miyauchi, S. Mouri, A. H. Castro Neto, K. Matsuda, and G. Eda, "Evidence for fast interlayer energy transfer in $MoSe_2/WS_2$ heterostructures," Nano Lett. **16**(7), 4087–4093 (2016).
13. H. Li, X. Zheng, Y. Liu, Z. Zhang, and T. Jiang, "Ultrafast interfacial energy transfer and interlayer excitons in the monolayer $WS_2/CsPbBr_3$ quantum dot heterostructure," Nanoscale **10**(4), 1650–1659 (2018).
14. C. D. LaBoda, A. R. Lebeck, and C. L. Dwyer, "An optically modulated self-Assembled resonance energy transfer pass gate," Nano Lett. **17**(6), 3775–3781 (2017).
15. A. Borgia, M. B. Borgia, K. Bugge, V. M. Kissling, P. O. Heidarsson, C. B. Fernandes, A. Sottini, A. Soranno, K. J. Buholzer, D. Nettels, B. B. Kragelund, R. B. Best, and B. Schuler, "Extreme disorder in an ultrahigh-affinity protein complex," Nature **555**(7694), 61–66 (2018).
16. W. Huang, P. Cheng, Y. M. Yang, G. Li, and Y. Yang, "High-performance organic bulk-heterojunction solar cells based on multiple-donor or multiple-acceptor components," Adv. Mater. **30**(8), 1705706 (2018).
17. C. Wang and E. A. Weiss, "Accelerating FRET between near-infrared emitting quantum dots using a molecular J-aggregate as an exciton bridge," Nano Lett. **17**(9), 5666–5671 (2017).
18. H. Zhu, Y. Fu, F. Meng, X. Wu, Z. Gong, Q. Ding, M. V. Gustafsson, M. T. Trinh, S. Jin, and X. Y. Zhu, "Lead halide perovskite nanowire lasers with low lasing thresholds and high quality factors," Nat. Mater. **14**(6), 636–642 (2015).
19. W. Li, Z. Wang, F. Deschler, S. Gao, R. H. Friend, and A. K. Cheetham, "Chemically diverse and multifunctional hybrid organic-inorganic perovskites," Nat. Rev. Mat. **2**(3), 16099 (2017).
20. D. Shi, V. Adinolfi, R. Comin, M. Yuan, E. Alarousu, A. Buin, Y. Chen, S. Hoogland, A. Rothenberger, K. Katsiev, Y. Losovyj, X. Zhang, P. A. Dowben, O. F. Mohammed, E. H. Sargent, and O. M. Bakr, "Solar cells. Low trap-state density and long carrier diffusion in organolead trihalide perovskite single crystals," Science **347**(6221), 519–522 (2015).
21. D. Gui, L. Ji, A. Muhammad, W. Li, W. Cai, Y. Li, X. Li, X. Wu, and P. Lu, "Jahn–Teller effect on framework flexibility of hybrid organic–inorganic perovskites," J. Phys. Chem. Lett. **9**(4), 751–755 (2018).
22. X. Yang, X. Zhang, J. Deng, Z. Chu, Q. Jiang, J. Meng, P. Wang, L. Zhang, Z. Yin, and J. You, "Efficient green light-emitting diodes based on quasi-two-dimensional composition and phase engineered perovskite with surface passivation," Nat. Commun. **9**(1), 570 (2018).
23. G. Jia, Z.-J. Shi, Y.-D. Xia, Q. Wei, Y.-H. Chen, G.-C. Xing, and W. Huang, "Super air stable quasi-2D organic-inorganic hybrid perovskites for visible light-emitting diodes," Opt. Express **26**(2), A66–A74 (2018).
24. C. Ran, J. Xi, W. Gao, F. Yuan, T. Lei, B. Jiao, X. Hou, and Z. Wu, "Bilateral interface engineering toward efficient 2D–3D bulk heterojunction tin halide lead-free perovskite solar cells," ACS Energy Lett. **3**(3), 713–721 (2018).
25. J. Liu, Y. Xue, Z. Wang, Z. Q. Xu, C. Zheng, B. Weber, J. Song, Y. Wang, Y. Lu, Y. Zhang, and Q. Bao, "Two-dimensional $CH_3NH_3PbI_3$ perovskite: synthesis and optoelectronic application," ACS Nano **10**(3), 3536–3542 (2016).
26. F. Ledee, G. Trippe-Allard, H. Diab, P. Audebert, D. Garrot, J.-S. Lauret, and E. Deleporte, "Fast growth of monocrystalline thin films of 2D layered hybrid perovskite," CrystEngComm **19**(19), 2598–2602 (2017).
27. Q. Liao, K. Hu, H. Zhang, X. Wang, J. Yao, and H. Fu, "Perovskite microdisk microlasers self-assembled from solution," Adv. Mater. **27**(22), 3405–3410 (2015).
28. D. Ma, Y. Fu, L. Dang, J. Zhai, I. A. Guzei, and S. Jin, "Single-crystal microplates of two-dimensional organic–inorganic lead halide layered perovskites for optoelectronics," Nano Res. **10**(6), 2117–2129 (2017).
29. H. Lu, H. Zhang, S. Yuan, J. Wang, Y. Zhan, and L. Zheng, "An optical dynamic study of $MAPbBr_3$ single crystals passivated with $MAPbCl_3/I_3$-$MAPbBr_3$ heterojunctions," Phys. Chem. Chem. Phys. **19**(6), 4516–4521 (2017).
30. W. Liu, J. Xing, J. Zhao, X. Wen, K. Wang, P. Lu, and Q. Xiong, "Giant two-photon absorption and its saturation in 2D organic-inorganic perovskite," Adv. Opt. Mater. **5**(7), 1601045 (2017).
31. L. Wang, I. Meric, P. Y. Huang, Q. Gao, Y. Gao, H. Tran, T. Taniguchi, K. Watanabe, L. M. Campos, D. A. Muller, J. Guo, P. Kim, J. Hone, K. L. Shepard, and C. R. Dean, "One-dimensional electrical contact to a two-dimensional material," Science **342**(6158), 614–617 (2013).
32. A. A. Lutich, G. Jiang, A. S. Susha, A. L. Rogach, F. D. Stefani, and J. Feldmann, "Energy transfer versus charge separation in type-II hybrid organic-inorganic nanocomposites," Nano Lett. **9**(7), 2636–2640 (2009).
33. D. M. Jang, D. H. Kim, K. Park, J. Park, J. W. Lee, and J. K. Song, "Ultrasound synthesis of lead halide perovskite nanocrystals," J. Mater. Chem. C Mater. Opt. Electron. Devices **4**(45), 10625–10629 (2016).
34. F. T. Rabouw, S. A. den Hartog, T. Senden, and A. Meijerink, "Photonic effects on the Förster resonance energy transfer efficiency," Nat. Commun. **5**(1), 3610 (2014).
35. S. Brittman and E. C. Garnett, "Measuring n and k at the microscale in single crystals of $CH_3NH_3PbBr_3$ perovskite," J. Phys. Chem. C **120**(1), 616–620 (2016).
36. S. J. Zhang, P. Audebert, Y. Wei, A. Al Choueiry, G. Lanty, A. Brehier, L. Galmiche, G. Clavier, C. Boissiere, J. S. Lauret, and E. Deleporte, "Preparations and characterizations of luminescent two dimensional organic-inorganic perovskite semiconductors," Materials (Basel) **3**(5), 3385–3406 (2010).
37. J. T. Li, S. K. Cushing, F. K. Meng, T. R. Senty, A. D. Bristow, and N. Q. Wu, "Plasmon-induced resonance energy transfer for solar energy conversion," Nat. Photonics **9**(9), 601–607 (2015).
38. Y. M. Kang, B. W. Li, and Z. Y. Fang, "Radiative energy transfer from MoS2 excitons to surface plasmons," J. Opt. **19**, 124009 (2017).

Optics EXPRESS

39. Y. Liu, H. Li, X. Zheng, X. Cheng, and T. Jiang, "Giant photoluminescence enhancement in monolayer WS2 by energy transfer from CsPbBr3 quantum dots," Opt. Mater. Express **7**(4), 1327 (2017).
40. S. Luo, X. Ma, H. Xie, M. Li, Y. Zhou, W. Cao, and P. Lu, "Controlling nonsequential double ionization of Ne with parallel-polarized two-color laser pulses," Opt. Express **26**(10), 13666–13676 (2018).
41. Y. Fang, H. Wei, Q. Dong, and J. Huang, "Quantification of re-absorption and re-emission processes to determine photon recycling efficiency in perovskite single crystals," Nat. Commun. **8**, 14417 (2017).
42. W. Liu, X. Li, Y. Song, C. Zhang, X. Han, H. Long, B. Wang, K. Wang, and P. Lu, "Cooperative enhancement of two-photon-absorption-induced photoluminescence from a 2D perovskite-microsphere hybrid dielectric structure," Adv. Funct. Mater. **2018**, 1707550 (2018).
43. H. Tsai, R. Asadpour, J.-C. Blancon, C. C. Stoumpos, O. Durand, J. W. Strzalka, B. Chen, R. Verduzco, P. M. Ajayan, S. Tretiak, J. Even, M. A. Alam, M. G. Kanatzidis, W. Nie, and A. D. Mohite, "Light-induced lattice expansion leads to high-efficiency perovskite solar cells," Science **360**(6384), 67–70 (2018).

1. Introduction

Semiconductor heterostructures, composed by stacking of various semiconductor layers, has provided a versatile tool to engineer the band structure [1–3] and design novel optoelectronic devices [4–6]. During the past years, interlayer charge transfer in semiconductor heterostructures has attracted lots of attentions due to the ultrafast dynamics and great tunability [7–11]. However, the low charge transfer efficiency has seriously hindered the practical applications of semiconductor heterostructures. Energy transfer is also commonly observed in semiconductor heterostructures, particularly when the emission spectrum of one component (donor) is overlapped with the absorption spectrum of the other component (acceptor) [12, 13]. The energy of an excited donor can travel across the interface and interact with the acceptor, which shows great promise for the practical applications in fluorescent sensors, solar cells and light-emitting diodes (LEDs) [14–17].

Recently, organic-inorganic perovskites have been intensively studied due to their excellent optoelectronic properties, such as high-absorption coefficient, low-defect density and long-carrier diffusion [18–20]. However, most of the previous reports mainly focused on the optoelectronic properties of individual perovskite components [21–23]. This issue has seriously limited the study and development of integrated perovskite nanodevices. Moreover, organic-inorganic perovskites have a high quantum yield for carrier generation, which provides an ideal candidate for high-efficiency heterostructures [24, 25]. Therefore, revealing the interlayer interaction of perovskite heterostructures is essential.

In this work, we perform a systematical study on the energy transfer in organic-inorganic perovskite heterostructure. The perovskite heterostructure is prepared by stacking the flakes of two perovskites $(PEA)_2PbI_4$ and $MAPbBr_3$. Under two-photon excitation, the photoluminescence (PL) emission of the $MAPbBr_3$ microplate is largely increased, while that of the $(PEA)_2PbI_4$ flake is completely quenched. Further study indicates that the opposite variation character of the PL emissions is originated from the radiative energy transfer from the $(PEA)_2PbI_4$ flake to the $MAPbBr_3$ microplate. The radiative energy transfer occurs on an ultrafast timescale with a high efficiency (~100%). In addition, the case under one-photon excitation is investigated for comparison, and a thickness- and wavelength-dependent interlayer interaction is observed.

2. Experiments and results

$(PEA)_2PbI_4$ monocrystalline films were synthesized by an anti-solvent vapor-assisted capping crystallization (AVCC) method [26]. After that, $(PEA)_2PbI_4$ flakes were obtained by mechanically exfoliating the monocrystalline films with a scotch tape. $MAPbBr_3$ microplates were prepared by a solution based self-assembly method [27]. Figure 1(a) and Fig. 1(b) show the optical microscope images of a $(PEA)_2PbI_4$ flake and a $MAPbBr_3$ microplate, respectively. Both of the two samples have a size over several ten micrometers. The uniform surfaces indicate a good crystallinity quality of the two perovskites. Figure 1(c) presents the XRD patterns of the two perovskite monocrystallines. The well-defined diffraction peaks of the XRD patterns correspond to the (00*l*) and (*h*00) series for $(PEA)_2PbI_4$ and $MAPbBr_3$

Optics EXPRESS

respectively, which agree well with the reported results [28–30]. To study the optical properties of the heterostructure composed of $(PEA)_2PbI_4$ and $MAPbBr_3$, a $(PEA)_2PbI_4$ flake and a $MAPbBr_3$ microplate were stacked together by a dry-transfer method [31]. Figure 1(d) shows the microscope image of a prepared perovskite heterostructure, in which the two perovskite components are well stacked, as labeled by the dashed lines. Figure 1(e) shows the normalized absorption spectrum of $MAPbBr_3$ (red curve) and PL spectrum of $(PEA)_2PbI_4$ (green curve), respectively. Since these two spectra are well overlapped, an efficient energy transfer can occur in the perovskite heterostructure [32].

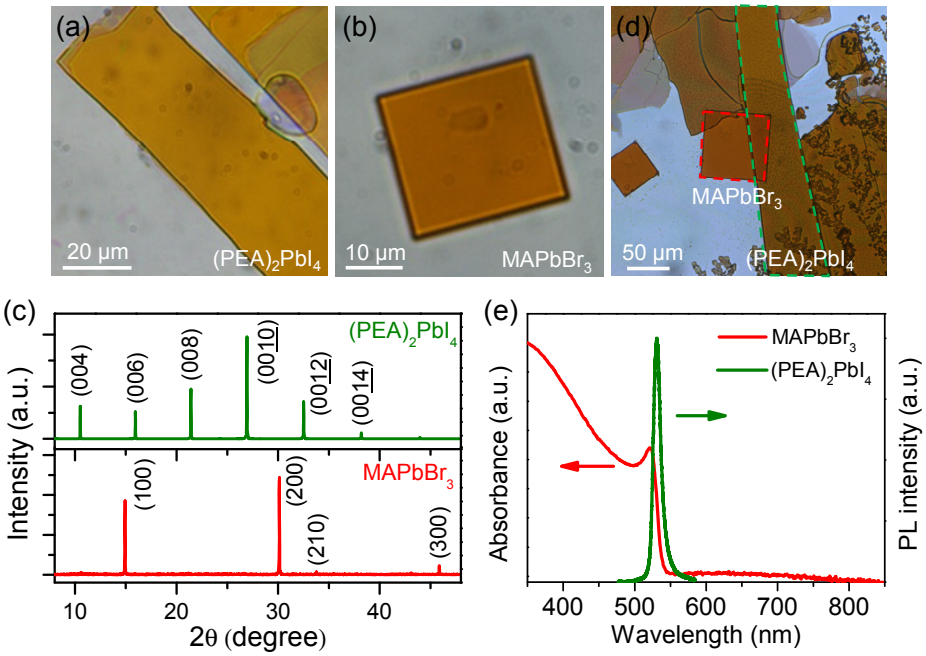

Fig. 1. Optical microscope images of (a) a mechanically exfoliated $(PEA)_2PbI_4$ flake and (b) a $MAPbBr_3$ microplate. (c) XRD patterns of the prepared $(PEA)_2PbI_4$ (up panel) and $MAPbBr_3$ (bottom panel) monocrystallines, respectively. (d) Optical microscope image of a prepared perovskite heterostructure. (e) Normalized absorption spectrum of $MAPbBr_3$ (red curve) and PL spectrum of $(PEA)_2PbI_4$ (green curve), respectively.

For further investigation, an inverted-confocal-microscope configuration was used for optical measurements, as shown in Fig. 2(a). A mode-locked Ti/Sapphire oscillator (Vitara, 800 nm, ~8 fs, 80 MHz) was used as the pumping source. The laser beam was focused onto the samples by a 20 × objective (Olympus, NA = 0.4). The reflected signals were collected by the same objective, and then sent to a spectrometer (ANDOR 193i) for spectral measurement or to a CCD camera for imaging. A time-correlated single-photon counting (TCSPC) system (Picoquant, PicoHarp 300) was equipped behind the spectrometer for time-resolved PL (TRPL) measurement. Figure 2(b) presents the PL spectra for the bare $(PEA)_2PbI_4$ flake (green curve), the bare $MAPbBr_3$ microplate (blue curve) and the heterostructure (red curve) under 800-nm excitation, respectively. The PL spectrum of the heterostructure was measured with the $MAPbBr_3$ microplate impinging the laser beam (forward excitation), as shown in the inset of Fig. 2(b). As the bandgaps of the two perovskites are larger than the one-photon energy (1.55 eV) but smaller than the two-photon energy (3.1 eV) of the pumping laser, the emissions are attributed to two-photon-absorption-induced PL (TPL). Figure 2(b) shows that the TPL intensity of the $(PEA)_2PbI_4$ flake is much stronger than that of the $MAPbBr_3$ microplate under the same excitation. For the perovskite heterostructure, the TPL emission of the $(PEA)_2PbI_4$ flake is nearly completely quenched, while that of the $MAPbBr_3$ microplate is

Optics EXPRESS

greatly increased (6.5 folds higher) in the heterostructure area. In addition, the TPL emission from the heterostructure has a redshift relative to that of the bare $MAPbBr_3$ microplate. Figure 2(c) shows the integrated TPL mapping of the perovskite heterostructure. A similar result is obtained that the integrated TPL intensity from the heterostructure area is decreased relative to that of the $(PEA)_2PbI_4$ flake, but it is largely increased relative to that of the $MAPbBr_3$ microplate. The opposite variation character of the TPL emission in the heterostructure indicates a strong interlayer interaction between the $(PEA)_2PbI_4$ flake and $MAPbBr_3$ microplate.

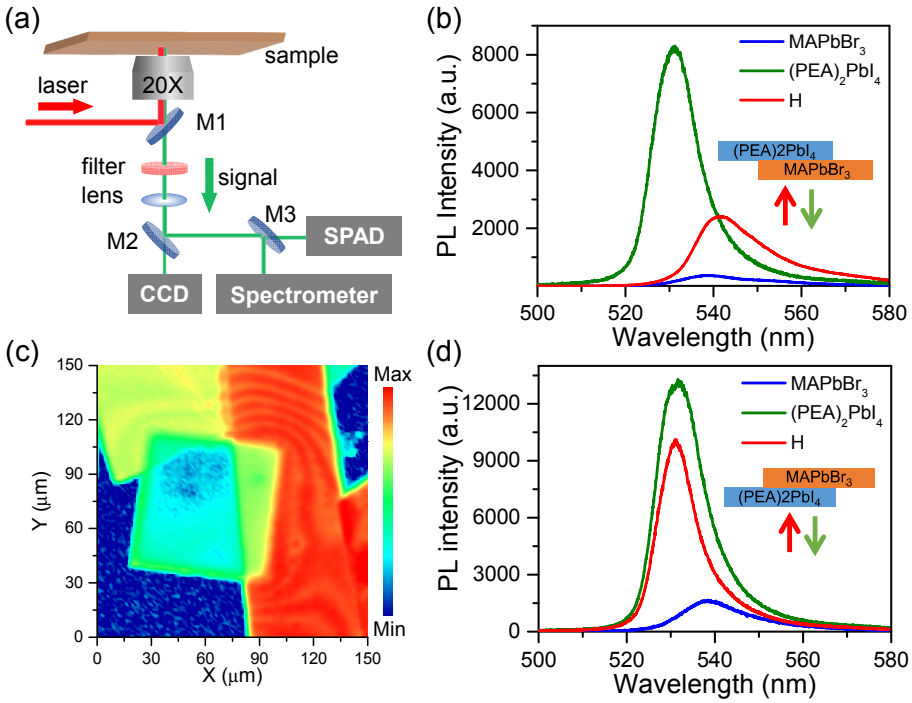

Fig. 2. (a) Schematic of an inverted-confocal-microscope configuration used for optical measurements. (b) Two-photon-absorption-induced PL (TPL) spectra of the $MAPbBr_3$ microplate, the $(PEA)_2PbI_4$ flake and the perovskite heterostructure (H) under forward excitation. (c) Integrated PL mapping of the perovskite heterostructure under forward excitation. (d) TPL spectra of the $MAPbBr_3$ microplate, the $(PEA)_2PbI_4$ flake and the perovskite heterostructure (H) under backward excitation.

For comparison, the interlayer interaction is studied with the $(PEA)_2PbI_4$ flake impinging the laser beam (backward excitation). Figure 2(d) shows the measured TPL spectra for the two perovskite components and heterostructure. In this case, the TPL spectrum from the heterostructure is similar to that of the bare $(PEA)_2PbI_4$ flake, which indicates a weak interlayer interaction between the $(PEA)_2PbI_4$ flake and $MAPbBr_3$ microplate. The difference in the TPL spectra of the perovskite heterostructure between forward and backward excitations implies that the interlayer interaction has a specific direction from the $(PEA)_2PbI_4$ flake to the $MAPbBr_3$ microplate.

It has been well known that two typical processes exist in the semiconductor heterostructures: energy transfer and charge transfer. Since the emission spectrum of $(PEA)_2PbI_4$ is strongly overlapped with the absorption spectrum of $MAPbBr_3$, the emitted energy of the $(PEA)_2PbI_4$ flake can travel across the interface and transfer to the $MAPbBr_3$ microplate, as illustrated in Fig. 3(a). As a result, the TPL emission of the $(PEA)_2PbI_4$ flake will be largely decreased, and that of the $MAPbBr_3$ microplate will be greatly increased.

Besides, the energy bands of the two perovskites exhibit a type-II band alignment, indicating a possible charge transfer process in the perovskite heterostructure, as shown in Fig. 3(b). However, it is worth noting that the lattice constants are ~8.68 Å and ~5.90 Å for $(PEA)_2PbI_4$ and $MAPbBr_3$ respectively, which indicates a large lattice mismatch between the two perovskites [28, 33]. This mismatch makes it difficult for the two perovskite components to couple via interlayer charge transfer at the interface. For further demonstration, a heterostructure composed of $MAPbBr_3/SiO_2/(PEA)_2PbI_4$ was prepared by depositing a SiO_2 dielectric layer (5 nm in thickness) on the $MAPbBr_3$ microplate. The SiO_2 layer will completely prevent the charge transfer between the two perovskite components. Figure 3(c) shows the TPL spectra for the two individual perovskite components and the heterostructure, respectively. Notably, the TPL emission of the $(PEA)_2PbI_4$ flake is completely quenched, and that of the $MAPbBr_3$ microplate is largely increased. The result is similar to that of the $MAPbBr_3/(PEA)_2PbI_4$ heterostructure, implying that the possibility of charge transfer can be eliminated. In addition, the variation of the dielectric environment from the individual perovskite components to the heterostructure may also have influence on the PL emission [34]. However, the contribution is quite limited because only a small dielectric mismatch exists between the $(PEA)_2PbI_4$ and $MAPbBr_3$ [35, 36]. Therefore, we can conclude that the energy transfer is a dominant process in the perovskite heterostructure.

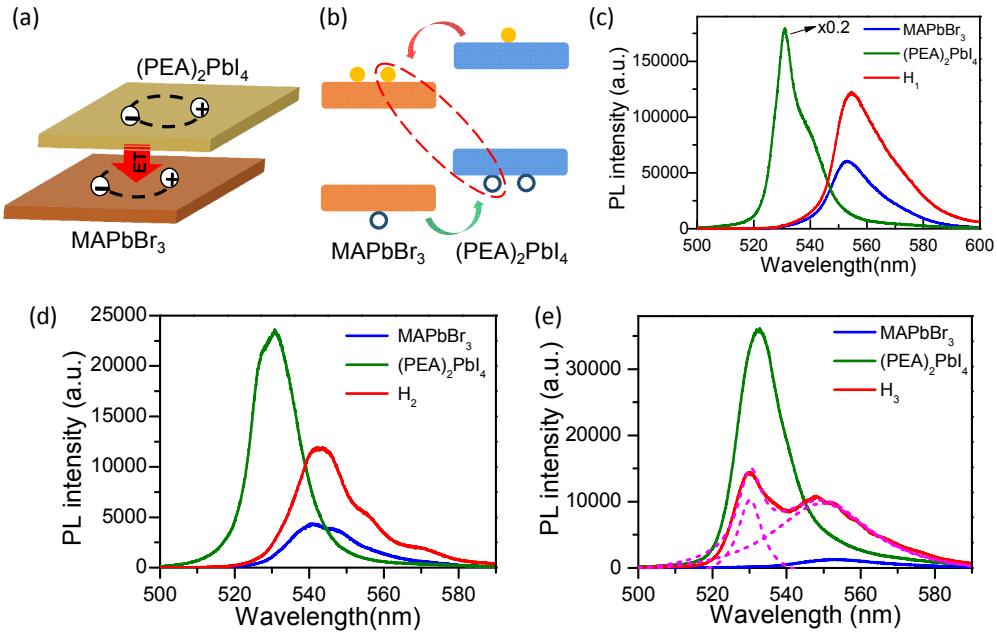

Fig. 3. (a) Schematic of energy transfer from the excited $(PEA)_2PbI_4$ flake to the $MAPbBr_3$ microplate. (b) Schematic of band alignment of $(PEA)_2PbI_4$ and $MAPbBr_3$, showing a type-II band alignment. TPL spectra of the individual components and the heterostructures (c) separated by a 5-nm-thick dielectric layer (H_1), (d) separated by a 10-nm-thick dielectric layer (H_2), and (e) separated by a 400-μm-thick dielectric layer (H_3), respectively, under forward excitation.

The nonradiative energy transfer such as Förster resonance energy transfer (FRET) and Dexter transfer are originated from the dipole-dipole interaction in the donor and acceptor, which strongly depends on the distance between the two components [37]. While the radiative energy transfer occurs in the form of photon radiation and absorption, which can still be efficient in a large distance [38]. To further distinguish these two processes in the perovskite heterostructure, the TPL emission of more samples separated by a thicker (100 nm) dielectric layer were measured. Figure 3(d) shows that The TPL emission of the $(PEA)_2PbI_4$ flake is

Optics EXPRESS

also completely quenched, and that of the $MAPbBr_3$ microplate is increased. As the nonradiative energy transfer can hardly occur with such a thick dielectric layer, the variation of the TPL emission in the perovskite heterostructure can be only attributed to the radiative energy transfer, which agrees will with the overlap of the emission spectrum of $(PEA)_2PbI_4$ and absorption spectrum of $MAPbBr_3$. Moreover, Fig. 3(e) shows the result for a heterostructure sample separated by a 400-μm-thick dielectric layer. The emission spectrum of the heterostructure is composed of two components from both of the $(PEA)_2PbI_4$ flake and $MAPbBr_3$ microplate. A part of the emission from the $(PEA)_2PbI_4$ flake is quenched, and also leads to the increase of the emission from the $MAPbBr_3$ microplate, indicating that the radiative energy transfer in the micro/nanostructures can still occur efficiently at a very long distance.

To get further insights into the energy transfer dynamics of the perovskite heterostructure, TRPL were measured using a TCSPC system under 800 nm excitation. Figure 4(a) shows the decay traces of the $(PEA)_2PbI_4$ flake, the $MAPbBr_3$ microplate and the perovskite heterostructure respectively. For the $(PEA)_2PbI_4$ flake, the decay trace can be fitted to a bi-exponential decay function, with two lifetimes of 0.61 ns and 2.46 ns respectively. These two decay channels correspond to the radiative recombination and the trap-assisted recombination, respectively. For the $MAPbBr_3$ microplate, the decay trace can be fitted to a single-exponential decay function, and a long lifetime of 5.53 ns is obtained. For the perovskite heterostructure, the decay time of the donor in the presence (τ_D) and absence (τ^0_D) of energy transfer obeys the following equation [32, 39]:

$$\frac{1}{\tau_D}=\frac{1}{\tau_D^0}+k_T \tag{1}$$

where k_T is the transfer rate. Figure 4(b) shows that the decay trace of the heterostructure starts nearly simultaneously with that of the $(PEA)_2PbI_4$ flake. The time contrast between these two processes (red and green curves) is beyond the resolution of the TCSPC system (~50 ps), indicating a ultrafast energy transfer rate ($k_T>>1/\tau^0_D$) from the $(PEA)_2PbI_4$ flake to the $MAPbBr_3$ microplate. Further, the energy transfer efficiency can be calculated to be [32]:

$$\Phi_T=1-\frac{\tau_D}{\tau_D^0}=\frac{k_T\tau_D^0}{1+k_T\tau_D^0}\approx 1. \tag{2}$$

The near-unity energy transfer efficiency is in good accordance with the TPL spectrum that the donor's emission is completely quenched in the perovskite heterostructure.

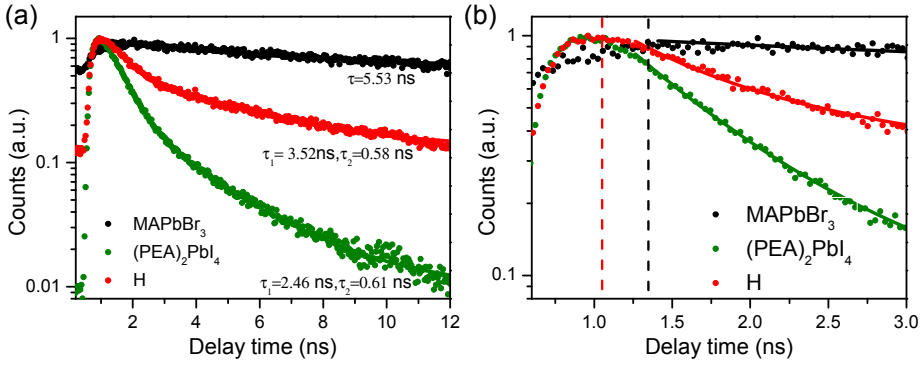

Fig. 4. (a) Time-resolved PL decay traces and the corresponding fitted results for the $MAPbBr_3$ microplate (black), the $(PEA)_2PbI_4$ flake (green) and the perovskite heterostructure (H) (red), respectively. (b) Enlarged PL decay traces shown in (a).

Optics EXPRESS

For comparison, the energy transfer process under one-photon excitation was investigated. A 400 nm laser was obtained by frequency doubling the laser beam of the Ti/Sapphire oscillator and used for excitation. Figures 5(a) and 5(b) show the PL spectra and decay traces for the bare perovskite components and heterostructure respectively, under forward excitation. Notably, the PL spectrum and the decay trace of the heterostructure are the same as those of the $MAPbBr_3$ microplate, indicating a weak interlayer interaction. As $MAPbBr_3$ has a strong absorption (k = 0.39) at 400 nm [35], the penetration depth is determined to be approximately 163 nm, which is much smaller than the actual thickness of the $MAPbBr_3$ microplate (> 1 μm). Consequently, the 400-nm laser beam can hardly transmit the $MAPbBr_3$ microplate to excite the $(PEA)_2PbI_4$ flake and no obvious energy transfer is observed. In contrast, with a thinner (215 nm) $MAPbBr_3$ microplate, the efficient energy transfer can also occur and lead to an increased PL emission of the acceptor, as shown in Fig. 5(c). For further confirmation, a 473 nm continuous-wave laser was used for excitation instead. The result is shown in Fig. 5(d). In this case, $MAPbBr_3$ has a smaller absorption of the laser beam (k = 0.22), and the energy transfer can be observed for the perovskite heterostructure with a thicker (420 nm) $MAPbBr_3$ microplate. Overall, the energy transfer process is strongly thickness- and wavelength-dependent under one-photon excitation, due to a much smaller penetration depth compared with that under two-photon excitation.

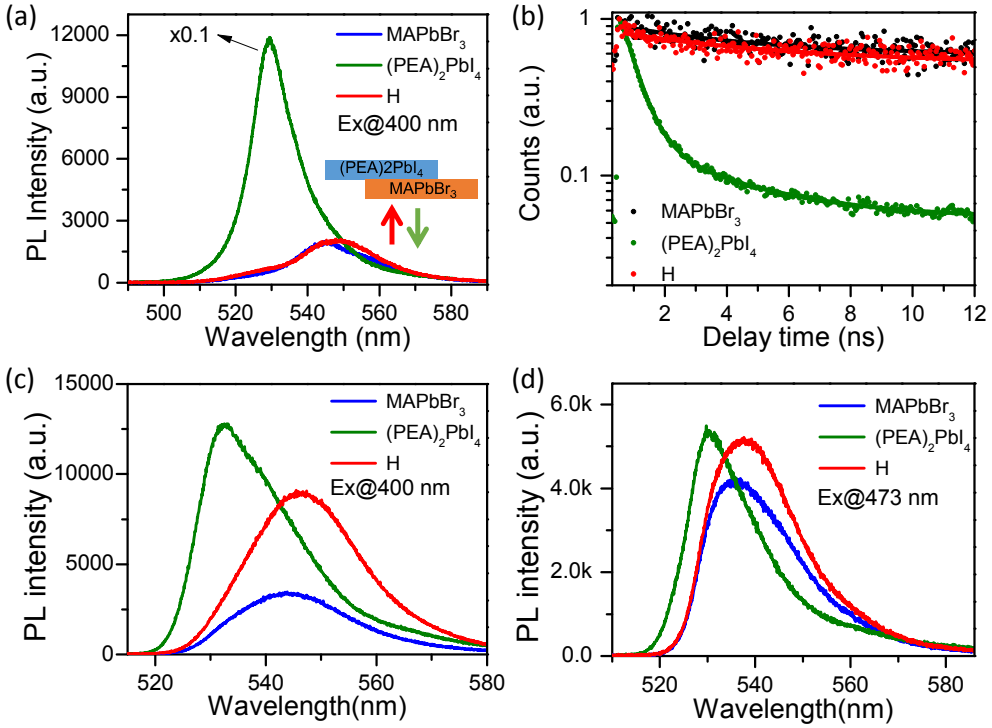

Fig. 5. (a) PL spectra and (b) decay traces for the individual perovskite components and heterostructure (H) respectively, under forward excitation at 400 nm. The thickness of the $MAPbBr_3$ microplate (> 1 μm) is much larger than the penetration depth of the laser beam (163 nm). (c) PL spectra for the individual perovskite components and heterostructure (H) with a 215-nm-thick $MAPbBr_3$ microplate, under forward excitation at 400 nm. (d) PL spectra for the individual perovskite components and heterostructure (H) with a 420-nm-thick $MAPbBr_3$ microplate, under forward excitation at 473 nm.

Optics EXPRESS

3. Conclusion

In conclusion, we study the energy transfer in perovskite heterostructure composed of $(PEA)_2PbI_4$ flake and $MAPbBr_3$ microplate in this work. Under two-photon excitation, the PL intensity of the $MAPbBr_3$ microplate can be greatly increased by about 6.5 folds, while the PL of the $(PEA)_2PbI_4$ flake was completely quenched in the heterostructure. The opposite variation of the PL intensity is attributed to the radiative energy transfer from the $(PEA)_2PbI_4$ flake to the $MAPbBr_3$ microplate. Further investigation indicates that the energy transfer occurs on an ultrafast timescale with a high efficiency (~100%), and the radiative energy transfer can overcome the distance limitation of the nonradiative energy transfer. In addition, a strongly thickness- and wavelength-dependent energy transfer is observed under one-photon excitation. This work has performed a direct investigation on the interlayer interaction of perovskite heterostructures. As the radiative energy transfer is strongly dependent on the overlap of the absorption and emission spectra of the two components, our result has a broad scope for the similar heterostructures, which advocates great promise for understanding the interlayer interaction and improving the performance of the perovskite nanostructures. For practical applications like optoelectronic detection and energy harvesting, it is desirable to perform with a ultrafast and efficient response [40–43]. The ultrafast and high-efficiency energy transfer in the perovskite heterostructures will have considerable potential for high-performance optoelectronic devices.

Funding

973 Programs (2014CB921301); National Natural Science Foundation of China (11204097 and 11674117); Doctoral Fund of Ministry of Education of China (20130142110078).

Acknowledgments

We acknowledge the Analytical & Testing Center of Huazhong University of Science and Technology (HUST) for XRD measurement.